In Vivo Imaging of Bioluminescent *Mycobacterium ulcerans*: A Tool to Refine the Murine Buruli Ulcer Tail Model

Till F. Omansen,[1,2] Renee A. Marcsisin,[1] Brendon Y. Chua,[1] Weiguang Zeng,[1] David C. Jackson,[1] Jessica L. Porter,[1] Ymkje Stienstra,[2] Tjip S. van der Werf,[2,3] and Timothy P. Stinear[1]*

[1]*Department of Microbiology and Immunology, The Peter Doherty Institute for Infection and Immunity, University of Melbourne, Parkville, Australia;* [2]*Department of Internal Medicine/Infectious Diseases, University Medical Center Groningen, University of Groningen, Groningen, The Netherlands;* [3]*Department of Pulmonary Diseases and Tuberculosis, University Medical Center Groningen, University of Groningen, Groningen, The Netherlands*

Abstract. Buruli ulcer (BU) is a neglected tropical disease caused by infection with *Mycobacterium ulcerans*. Unclear transmission, no available vaccine, and suboptimal treatment regimens hamper the control of this disease. Carefully designed preclinical research is needed to address these shortcomings. In vivo imaging (IVIS®, Perkin Elmer, Waltham, MA) of infection is an emerging tool that permits monitoring of disease progression and reduces the need to using large numbers of mice at different time-points during the experiment, as individual mice can be imaged at multiple time-points. We aimed to further describe the use of in vivo imaging (IVIS) in BU. We studied the detection of *M. ulcerans* in experimentally infected BALB/c mouse tails and the subsequent histopathology and immune response in this pilot study. IVIS-monitoring was performed weekly in ten infected BALB/c mice to measure light emitted as a proxy for bacterial load. Nine of 10 (90%) BALB/c mice infected subcutaneously with 3.3×10^5 *M. ulcerans* JKD8049 (containing pMV306 hsp16+luxG13) exhibited light emission from the site of infection, indicating *M. ulcerans* growth in vivo, whereas only five of 10 (50%) animals developed clinical signs of the disease. Specific antibody titers were detected within 2 weeks of the infection. Interferon (IFN)-γ and interleukin (IL)-10 were elevated in animals with pathology. Histopathology revealed clusters of acid-fast bacilli in the subcutaneous tissue, with macrophage infiltration and granuloma formation resembling human BU. Our study successfully showed the utility of *M. ulcerans* IVIS monitoring and lays a foundation for further research.

INTRODUCTION

Mycobacterium ulcerans causes the neglected tropical disease Buruli ulcer (BU) that can manifest as a skin nodule, plaque, edematous lesion, or open skin ulcer characterized by yellowish-white necrosis and undermined edges.[1] The disease generally occurs in clustered foci in rural Central and Western Africa but also has gained prominence in specific regions of southeast Australia. Presently, 12 countries actively report BU cases to the WHO and 33 have ever reported cases.[2] Patients with BU suffer from stigmatization, social participation restrictions, and physical disability long after treatment is completed.[3] The main pathogenic factor in BU is a diffusible cytotoxin called mycolactone (ML). Mycolactone is a polyketide-derived macrolide that is responsible for the pathological triad of necrosis, suppressed local inflammatory response, and hypoalgesia of the lesion.[4,5] Mycolactone suppresses an efficient host innate and adaptive immune response by means of preventing protein translocation into the endoplasmic reticulum.[6,7] The 174-kb large plasmid pMUM001 is responsible for ML production by *M. ulcerans*.[8]

There are several major challenges to controlling BU, such as the unclear mode(s) of transmission, imperfect treatment regimens, and the lack of a rapid diagnostic test. The mode of transmission is poorly understood and seems to vary by geographic location, although puncturing injuries after contamination from an environmental source seem to be at least one likely route of infection.[9,10] In southeast Australia, mosquitoes have been linked to transmission.[11,12] Buruli ulcer is presently treated with an 8-week regimen of rifampin and streptomycin, or a regimen where the injectable streptomycin is replaced with clarithromycin after 4 weeks; a fully oral, 8-week rifampin and clarithromycin regimen has been trialed in humans, and the current trial analysis is ongoing (ClinicalTrials.gov Identifier: NCT01659437).[13,14] Progressed, larger lesions are often managed with antimicrobial treatment and, in addition, surgical excision of the infected tissue, followed by functional repair and skin grafting[15]; a recent study showed that the time-point for decision-making on whether to intervene surgically or not does not matter for overall healing outcomes.[16] No vaccine is available despite several efforts to use the Bacille Calmette Guerin (BCG) vaccine or to develop novel vaccines.[17] Hence, more preclinical research in *M. ulcerans* transmission, chemotherapy, and vaccination, as well as pathogenesis, is necessary to solve the biomedical challenges complicating BU infection control.

Mycobacterium ulcerans mouse infection models have been pivotal in guiding research and clinical studies regarding these questions in the past.[18–20] The mouse footpad infection and mouse tail infection are the two best established methods to study experimental infection with *M. ulcerans* in animals.[18,21] The footpad model has been derived from experience with experimental infection of *Mycobacterium leprae* in mice.[18,22] This model has been used in numerous preclinical studies, to mainly evaluate not only drug efficacy but also vaccines for *M. ulcerans*.[19,20,23–35] Tail infection has been used to study pathology and vector research[21] and vaccinology.[36] Given that BU is a subcutaneous (SC) infection mostly occurring on the lower and upper limbs in humans,[1,37] the mouse footpad and tail are obvious sites to model the disease. The absence of fur in mice at these sites allows for easy clinical observation; a lower temperature of the skin on extremities than on the core body has also been hypothesized to favor the growth of *M. ulcerans*, which in laboratory conditions grows best at 32°C. Tail infection offers a cutaneous

infection site that is not in contact with the environment as much as the footpad so that contamination, redistribution, or loss of inoculum and animal impairment in more advanced stages of the disease are less likely to occur. Also, it is a more practical region for imaging than the footpad.

Preclinical studies such as drug efficacy and vaccine research need to assess the bacterial burden in lesions at given time-points. The method of choice for this is enumeration of colony-forming units (CFUs) from mouse footpad homogenate[27,38]; to obtain footpad samples, subsets of mice have to be culled at every time-point. The use of bioluminescence as readout not only offers a reduction in sample size of such experiments but also allows us to refine the experiment because repeated measures can be taken non-invasively at many time-points in the same animal, whereas CFUs are always compared with different mice which are biological replicates.[30]

The use of bioluminescence represents a useful addition, or even an alternative to CFU enumeration as its assessment can be carried out without killing the animal, allowing for serial testing in the same animal and reduction in overall sample size. Bioluminescent strains of *M. ulcerans* have been previously used to evaluate drug efficacy in in vitro and in vivo *M. ulcerans*,[30,31,35,39] as well as in vector ecology studies.[10] Drug efficacy studies repurposed a luminometer for the readout of bioluminescence, an apparatus designed to measure luminescence from bacteria in test vials. In this study, we sought to test a more advanced and sensitive readout, namely, an in vivo imaging system (IVIS) for the imaging of bioluminescence from experimental murine *M. ulcerans* infection, all in the effort to further refine and reduce animal usage and aid the advance of the much needed preclinical BU research. The Lumina XRMS Series III IVIS camera (Perkin Elmer, Waltham, MA) used in this experiment has higher sensitivity than a luminometer. The IVIS camera also allows overlaying of a photographic image with the detected light signal to visualize and localize bacteria; a luminometer only produces the quantification. We hypothesized that the application of modern IVIS imaging technology allows us to thus sensitively detect bacteria when no outer clinical pathology is visible. An experimental low-burden infection with 3.3×10^5 CFU *M. ulcerans* was selected, anticipating that some animals might not display visible pathology, to test the sensitivity of the IVIS camera. The bioluminescent *M. ulcerans* strain used in this study has been previously described and contains the pMV306 hsp16+luxG13 reporter plasmid[39–41] that integrates into the mycobacterial chromosome and contains the lux operon (luxABCDE). Thus, it does not require the addition of an exogenous substrate to detect bioluminescence.[40] Besides the demonstration of *M. ulcerans* imaging of early to advanced lesions, we also compared their histopathological appearance with reports of human cases. The immune response to our bioluminescent *M. ulcerans* strain was assessed to establish a baseline for further model development, and subsequent vaccine and transmission research.

MATERIALS AND METHODS

Culture conditions. *Mycobacterium ulcerans* JKD8049 harboring pMV306 hsp16+luxG13 was grown on Middlebrook 7H10 agar or in 7H9 broth containing 10% oleic albumin dextrose catalase growth supplement (Middlebrook, Becton

Dickinson, Sparks, MD), 0.5% glycerol, and 25μg/mL kanamycin sulfate (Amresco, Solon, OH). Plates and flasks were incubated for 8–10 weeks at 30°C, 5% CO_2. Liquid chromatography–mass spectrometry was used to confirm that bioluminescent bacteria were still producing ML.[42]

Establishing a standard curve for bioluminescent *M. ulcerans* JKD8049. Light emission in photons/second was compared with CFUs for *M. ulcerans* JKD8049 cultured in Middlebrook 7H9 medium for 4 weeks and then diluted in serial 10-fold steps in 96-well trays. Photon emissions were captured using a Lumina XRMS Series III in vitro imaging system (IVIS) (Perkin Elmer, Waltham, MA). Bacterial CFUs were confirmed by the spot plate method.[10]

Mouse tail infections. Animal experimentation adhered to the Australian National Health and Medical Research Council Code for the Care and Use of Animals for Scientific Purposes and was approved by and performed in accordance with the University of Melbourne Animal Ethics Committee (Application: 1312756.1). The animals were purchased from ARC (Canning Vale, Australia). On arrival, animals acclimatized for 5 days. Food and water were given ad libitum. Ten 6-week-old, female BALB/c mice were inoculated with a low-burden dose of 3.3×10^5 *M. ulcerans* CFUs by SC injection into the dorsal aspect of the upper third of the tail. The concentration of the bacterial inocula was confirmed by spot plating. After 17 weeks postinoculation or whenever the humane endpoint was reached, mice were humanely killed.

In vivo imaging. Mice were imaged once a week during morning time using a Lumina XRMS Series III IVIS. During imaging, mice were anesthetized with 2.5% isoflurane gas (Ceva Animal Health, Glenorie, Australia). The stage on which the mice were placed during imaging was warmed to 37°C. Photon emissions were acquired with the following settings: exposure time 5 minutes, emission filter: open, excitation filter: blocked, binning: medium, F/stop 1. These images were superposed onto conventional black/white photographs (exposure time: auto, binning: medium, F/stop: 16). Images from the ventral and dorsal aspects of the tail were taken. Images were analyzed using Living Image® software (Perkin Elmer, Waltham, MA). Areas emitting light were defined as regions of interest (ROI). A copy of every ROI was placed next to those areas for background measurement. Photons per second from the ROIs were computed and values from background regions subtracted from the actual ROI. Results from ventral and dorsal images (Figure 1B) were added and the cumulative luminescence of the two imaging angles recorded.

ELISA. Blood samples were obtained by submandibular puncture and, at experimental endpoint, by cardiac puncture. Serum was collected by centrifugation and stored at −20°C. All incubation of ELISA plates was carried out in a moisturized container at room temperature. Flat-bottom polyvinyl chloride microtiter plates (Thermo Fischer, Milford, MA) were coated with 5 μg of the antigen overnight. Antigens used were the mycobacterial small heat-shock protein 18 (Hsp 18) and *M. ulcerans* whole cell lysate (WCL), prepared as previously described.[43,44] The antigen was discarded and plates blocked for 1 hour with phosphate buffered saline (PBS) containing 10 mg/mL bovine serum albumin. Plates were washed four times with PBS containing 0.05% Tween-20 (PBST). Sera were added in eight serial dilutions in PBS to the plate and incubated for 4 hours. Plates were washed with PBST again and 50 μL/well horseradish peroxidase-conjugated polyclonal rabbit anti-mouse Ig antibody (Dako,
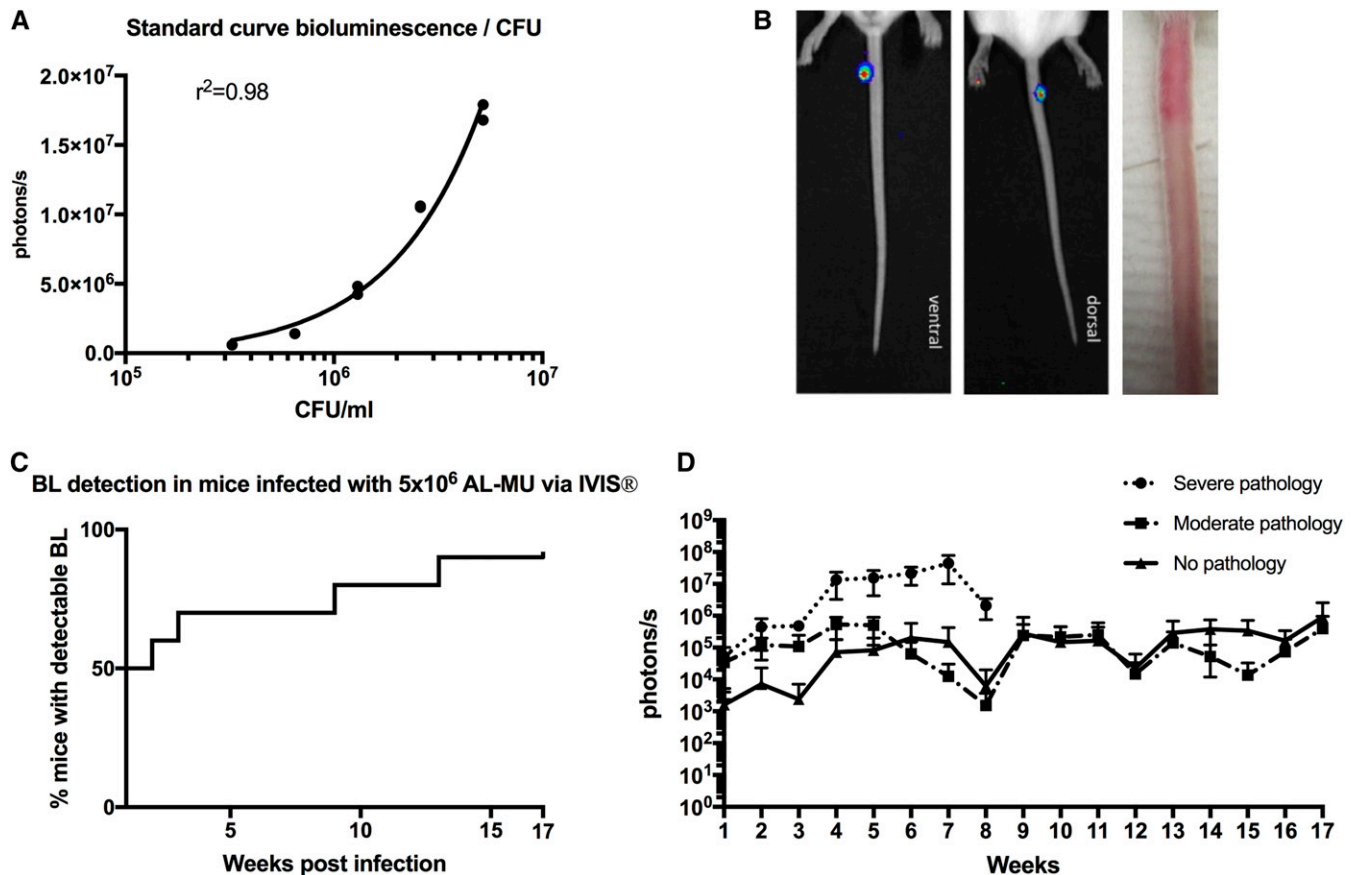
FIGURE 1. Use of bioluminescent *Mycobacterium ulcerans* to follow the evolution of disease in the mouse tail model of Buruli ulcer. (**A**) Standard curve comparing bioluminescence and colony-forming units (CFUs) of the *M. ulcerans* JKD8049+pMV306 hsp16 luxG13 reporter strain. (**B**) IVIS (left) and photographic images (right) from BALB/c mice infected via subcutaneous tail inoculation with approx. 3.3×10^5 CFU/mL *M. ulcerans* harboring the bioluminescent reporter plasmid. Photons/s emitted from bioluminescent bacteria were detected by IVIS in anesthetized mice. Results are represented in a pseudo-colored scheme (red indicated high, yellow indicated medium, and green indicated low intensity of the light emitted). Light was detected from both the dorsal (site of injection) and ventral aspects of the mouse tail. The photos were taken at 4 weeks postinfection; the bioluminescence readout was 1.8×10^6 photons, corresponding to approx. 6.7×10^5 CFU/mL according to our standard curve. (**C**) Survival graph representing time to detectable bioluminescence emission from mice infected with bioluminescent *M. ulcerans* into the tail (**D**) Development of mean photons/s emitted from mice infected with 3.3×10^5 bioluminescent *M. ulcerans* into the upper third of the dorsal tail. Values represent the mean of dorsal and ventral photons/s measurement. Animals were subgrouped for analysis by clinical staging based on severity of the gross pathology (severe: redness, swelling, edema, and impending ulceration; moderate: redness and edema; and no pathology). This figure appears in color at www.ajtmh.org.

Glostrup, Denmark) was added in a 1:400 dilution in PBS for 1 hour. Subsequently, ELISA substrate (0.2 mM 2,29-azino-bis 3-ethylbenzthiazoline-sulfonic acid in 50 mM citric acid containing 0.004% hydrogen peroxide) was added to detect bound antibodies. Absorbance was read in a plate reader at 405 nm and 450 nm, and the average of the two wavelengths was recorded.

Intracellular cytokine staining and fluorescence activated cell sorting. Dissected spleens were homogenized with a mesh (70 μm cell strainer, Miltenyi Biotech (Bergisch Gladbach, Germany) and treated with ammonium Tris chloride. Splenocytes (1×10^6) were restimulated with 2 μg *M. ulcerans* JKD8049 WCL in RPMI 1640 (Merck, Darmstadt, Germany) supplemented with 64 mM L-glutamine, 32 mM sodium pyruvate, 1.75 mM 2-mercaptoethanol, 3165 μg/mL penicillin (all Gibco® Life Technologies, Carlsbad, CA), 760 μg/mL gentamicin (G-Bioscience, St. Louis, MO), and 10% heat-inactivated fetal calf serum (CSL, Parkville, Australia) for 72 hours at 37°C, 5% CO_2. Sixty-nine-well, round-bottom plates (Corning Life Sciences, Corning, NY) were spun down, supernatant collected, and stored at –20°C.

Cytokines were stained using the bead-based Cytometric Bead Array Mouse Th1/Th2/Th17 Cytokine Kit (BD, North Ryde, Australia) according to the manufacturer's instructions. Samples were run on a BD FACSCanto™ II flow cytometry system (BD Biosciences, San Jose, CA) and data analyzed using FCAP Array™ analysis software version 3.0 (BD Biosciences, San Jose, CA).

Histology. A section ranging approx. 5 mm from the midline of the ulcer proximally was dissected and stored in 10% buffered formalin for histological assessment. Prepared paraffin blocks were surface-decalcified with 10% nitric acid for 5 minutes before cutting 4-μm sections. Hematoxylin and eosin (H&E) and Ziehl–Neelsen (ZN) staining were used following standard protocols. The specimens were subjected for analysis by an independent pathologist, who was blinded to the clinical extent of BU as well as to the bioluminescence results to reduce bias. Presence of acid-fast bacilli (AFB), inflammatory cells (macrophages, plasma cells/lymphocytes, neutrophils, and eosinophils) as well as the degree of inflammation (granulomas, panniculitis, calcification, vasculitis, and neuritis) and the tissue damage (dermal and fat tissue

necrosis, muscle layer involvement, and bone change), and the vascular involvement were scored. Specimens from two non-infected, naive mice were used as controls.

Statistical analysis. Statistical analysis was performed using GraphPad Prism version 7.0a (GraphPad Software, Inc., San Diego, CA). Bioluminescence data were plotted as arithmetic mean of the ventral and dorsal reading, as described earlier. Time to bioluminescence is displayed as survival curve. Antibody titers are represented as the reciprocal of the highest dilutions of serum needed to measure an absorbance value of 0.2. Data were transformed by plotting absorbance values versus the data of log 0.5—fold dilutions of each group, a nonlinear regression analysis was performed to obtain a line of best fit (with 95% CI) to which the intersect value of 0.2 was determined. One-way analysis of variance followed by a Tukey's multiple comparisons test assuming an alpha of 0.05 was used to test for statistical significant difference between antibody titer measurements. Cytokine readings are compared using descriptive statistics.

RESULTS

Standard curve comparing photon/s with CFU readout. To compare bioluminescence readout with actual bacterial burden, we first established a standard curve in vitro. We were able to interpolate a standard curve by nonlinear regression, showing a very high positive correlation ($r^2 = 0.98$) between photons/s and CFU/mL (Figure 1A).

Establishment of mouse tail infection. To evaluate virulence and to study murine infection, bioluminescent *M. ulcerans* was injected subcutaneously into mouse tails. The tail infection- resulted in 90% (nine of 10) of mice presenting measurable light emission on IVIS images. Other than at the injection site at the tail, no other foci of infection as indicated by bioluminescence was observed (Figure 1B). Fifty percent (five of 10) gradually developed macroscopically apparent lesions resembling BU within 17 weeks (Figure 1C). None of the animals showed other signs of illness than skin lesion that were restricted to the approximate sites of injection.

Course of the infection as measured by bioluminescence. To study the course of infection in terms of bacterial burden measured in bioluminescence, mice were imaged weekly with the IVIS system. Bioluminescence, measured in emitted photons/s, rose exponentially to a maximum of 1×10^7 in week 7 (Figure 1D). Compared with our in vitro–generated standard curve, this would equal to approx. 5×10^6 CFU/mL (Figure 1A) and was associated with advanced, severe pathology (Table 1). From this time point, the signal declined to a 1×10^5 (corresponding to 4×10^4 bacteria on the in vitro standard curve) threshold until the end of the experiment. At week 8, three mice reached the humane endpoint and were euthanized. In examining the antibody titer levels against *M. ulcerans* whole cell lysate, these began to rise in week 8, co-occurring with a decrease in photons/s counts. Animals displaying severe symptoms (swelling, redness and impeding ulceration, and scabbing of the tail) had higher photons/s counts, indicating higher bacterial burden, compared with those with moderate (redness and minor swelling) or no pathology. Photons/second counts increased per week until weeks 6–8, when the infection seemed to plateau.

Antibody titers. To characterize the antibody-mediated immune response to *M. ulcerans*, we obtained plasma samples for ELISA at weeks 2, 4, 8, 13, and 17 of the experiment.

TABLE 1
Overview of histopathological findings of mice subcutaneously infected with autoluminescent *Mycobacterium ulcerans* into the tail

Clinical picture	Identifier	Bioluminescence (in photons/s) area under the curve	Acid-fast bacilli	Inflammation	Tissue damage	Vascular involvement	Inflammatory cell type	Degree of inflammation
Severe pathology (sacrificed at week 8)	84	1.36E+08	++	+++	+++	n/a	PC, MФ, and LYM	Severe, multifocal, and chronic
	85	1.35E+08	+++	+++	+++	n/a	PC, MФ, LYM, and EOS	Severe, multifocal, and chronic
	88	1.72E+07	++	+++	+++	++	PC, MФ, and LYM	Severe, multifocal, and chronic
Moderate pathology	86	1.97E+06	-	+	+	+	MФ and LYM	Mild to moderate, chronic, and multifocal
	89	3.69E+06	+	+/++	++	++	PC and MФ	Mild, diffuse, and chronic
No macropathology	81	2.15E+06	-	+	+	-	MФ and LYM	Moderate, chronic, and focal
	82	692641	-	-	-	-	–	None
	83	872438	-	+	+	+	MФ and LYM	Moderate, chronic, and multifocal
	87	7.24E+06	++	+++	+++	++	PC, MФ, and LYM	Locally severe and chronic
	90	0	-	+	+	+	PC, MФ, EOS, and NEU	Mild, chronic, and multifocal

EOS = eosinophil; LYM = lymphocyte; MФ = macrophage; NEU = neutrophil; PC = plasma cell; n/a: not applicable. Animals were divided by clinical pathology: severe pathology, moderate pathology, and no macropathology. The amount of photos/second as a proxy for bacterial quantity correlated with pathology, except in mouse 87, where no clinical pathology was seen. Photons per second analyzed by IVIS imaging are shown in comparison with histological results.

Over time, there was a slight increase of antibody titers in response to *M. ulcerans* WCL, but overall, a late onset of the antibody response was noted (Figure 2A). Antibody titers reached higher levels between weeks 11 and 17 (Figure 2A). The response to *M. ulcerans* Hsp 18 and WCL was compared, and no statistically significant difference ($P > 0.05$) was found (Figure 2B). Furthermore, ELISA results in response to WCL at week 8 were compared between animals with severe, moderate, and no clinical pathology, and no statistically significant difference ($P > 0.05$) was found (Figure 2C and D).

Late suppression of cytokines. To characterize and study the cytokine profile in our murine *M. ulcerans* infection model, intracellular cytokine staining was performed on spleen samples after 8 and 17 weeks of the experiment, when three and seven mice were humanely killed, respectively. The cytokine concentrations in splenocyte samples restimulated with 2 μg *M. ulcerans* JKD8049 WCL were compared between mice with pathology culled at week 8 and those with and without pathology culled at week 17. In the three mice that were culled prematurely because of rapidly extending disease in week 8, elevated levels of IFN-γ and IL-10 were measured. Overall, cytokine levels were very low for all assayed cytokines in week 17, regardless of the clinical state of the animal (Figure 3).

Histopathology of lesions. To validate the model and study, the pathology of *M. ulcerans*, histopathology was performed on skin lesions and compared with those of humans described in the literature.[45,46] Specimens from infected tissue were subjected to histopathological analysis in ZN and H&E staining. Aggregates of AFB, *M. ulcerans*, were observed at 300–400 μm beneath the epidermis (Figure 4A). Furthermore, epidermal hyperplasia and immune cell infiltrates were apparent (Figure 4). Bioluminescence (photons/second) as proxy for bacterial quantity correlated well with the histological extent of disease, except for mouse ID 87 (Table 1). Numerous AFB as well as severe, multifocal, chronic inflammation marked by the presence of plasma cells, macrophages, and lymphocytes were observed in mice with severe clinical pathology. There was extensive tissue damage, as well as vascular involvement, in these animals. Mice with moderate clinical pathology exhibited mild and rather diffuse histological pictures and less tissue damage. Mice that had no obvious clinical signs of disease had low bioluminescence and showed moderate to little localized/focal histological features of inflammation (Table 1, Figure 4).

DISCUSSION

In this study, we have successfully shown the applicability of IVIS imaging of *M. ulcerans* in a low-burden experimental SC tail infection mouse model. The lesion histopathology correlated with previously reported human pathology. The use of bioluminescent *M. ulcerans* JKD8049 (pMV306 hsp16+luxG13) allowed the infection to be followed and characterization of host immune responses to *M. ulcerans* in BALB/c mice. The onset of clinical signs was gradual, and the mice developed characteristic, localized lesions. Necrosis of the subcutis, chronic inflammation with the presence of macrophages and lymphocytes, granuloma formation, panniculitis, as well as the presence of AFBs correlating with disease progression are hallmarks of BU histopathology described in humans.[47,48] The extent of and the overall pathology observed in the mouse tail tissue in our study were comparable with the aforementioned experience from human patients supporting the use of this mouse model to study BU.[45,46]

The bioluminescence readout correlated with the histopathological outcome in a dose-dependent manner, where an elevated photons/s count indicating high bacterial burden coincided with more progressive histological disease (Table 1) underlining the usefulness of IVIS imaging and bioluminescence as a marker for disease progression. Both clinically apparent and nonapparent lesions could be visualized with IVIS highlighting its sensitivity and usefulness in imaging early or low-burden infection. The use of bioluminescent *M. ulcerans* permitted us to also verify the location of the bacteria; after SC injection, we observed the presence of photon emission exclusively in the upper third of the mouse tail, which was the site of injection. This underlines the concept of BU as a localized infection, where disease manifestations only occur at the site of inoculation.

We approximated the growth rate in the lesion by comparison with an in vitro–derived standard curve. We noticed a
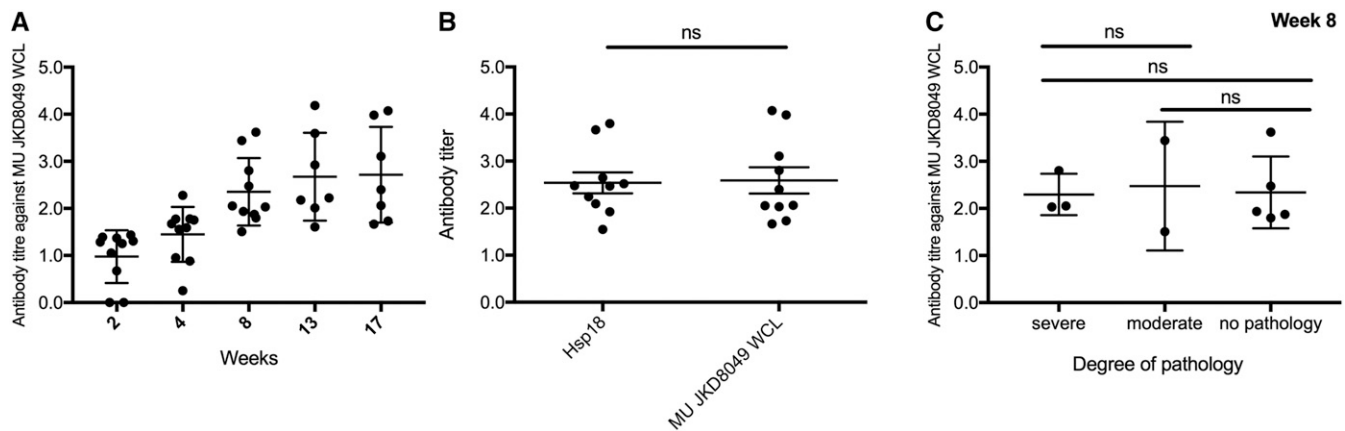

FIGURE 2. Evolution of the antibody titer against *Mycobacterium ulcerans* whole cell lysate (WCL) and small heat-shock protein 18 (Hsp18) measured in plasma from mice infected with *M. ulcerans* over time. A late onset of overall antibody response against an unspecific *M. ulcerans* WCL was noted in the bioluminescent *M. ulcerans* tail infection model. Antibody titers rose late, after 8 weeks, and plateaued at week 13 (**A**). No difference ($P > 0.5$) was observed in the antibody titer against small Hsp 18 and WCL (**B**). No statistical significance in antibody levels was seen between animals with severe, moderate, or no apparent pathology ($P > 0.5$; **C**).
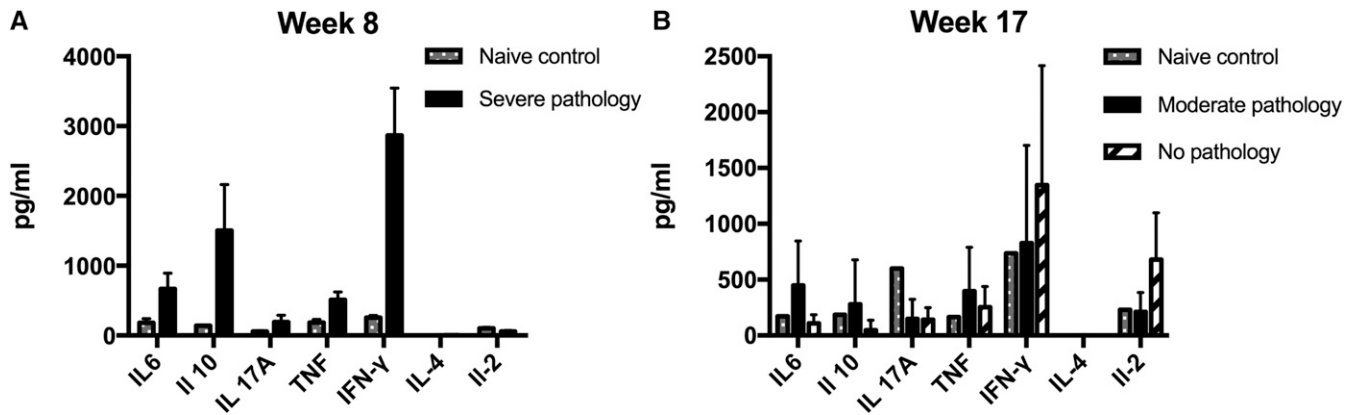
FIGURE 3. Comparison of cytokine profile assessed by intracellular cytokine staining of mice infected with bioluminescent *Mycobacterium ulcerans* after 8 (**A**) and 17 (**B**) weeks of infection to naive, noninfected mice. Error bars represent standard error of the mean. Mice with advanced clinical pathology sacrificed at week 8 of the experiment displayed highly elevated IFN-γ, as well as IL-6 and IL-10 levels (**A**). IFN-γ is known to activate macrophages and is a key regulator in granuloma formation in mycobacterial infections. At week 17, infected mice with no apparent pathology had higher IFN-γ counts than other mice, as well as slightly elevated IL-2 levels.

decline and plateauing of bioluminescence from week 8 onward. This phenomenon could be explained by a plateauing of the bacterial growth curve in the lesion and transition into a stationary phase where less of the immunosuppressive toxin ML is produced and partial host control is established. This latter conclusion is supported to some extent by the rise of antibody titers around that time point, also decreased transcription of the bioluminescence plasmid, and, hence, decreased luminescence could be an issue interfering with light emission (Figure 2). Vasculopathy is a feature of BUs observed in humans[47] and mice (Table 1, Figure 4). A hypoxic state within the lesion might also decrease bioluminescence, and more research is needed to elucidate the usefulness of bioluminescence as a marker of bacterial quantity beyond approx. 8 weeks of infection in the BALB/c mouse. Overall, IVIS imaging of *M. ulcerans* had been applied in one study before this, where it was used as a readout in transmission research examining different routes of infection, for example, mosquito bite or needle stick trauma.[10] In this pilot study, we developed this idea further and tested IVIS imaging of experimentally infected mice with the aim to refine the mouse tail model of BU and to create a baseline knowledge of host immune response to the autoluminescent strain for subsequent vaccine studies.

Immunology and course of disease. The immune response to *M. ulcerans* is influenced by the microbes' toxin, ML. Dendritic cells are inhibited by ML, which can impair their ability to prime cellular immune responses and phagocytose the bacteria.[49] Also, suppression of a CD4+ immune response was observed in humans[50,51] and efficient mounting of a Th1 response and elevated IFN-γ seemed protective.[52] T-cell depletion, mediated by miRNAs, has also been attributed to ML.[53] It is believed that, like in tuberculosis, an effective cell-mediated immune response can naturally control the infection and is likely also important for conferring transient protection against BU, experimentally.[54] Markedly elevated cytokines in human Buruli cases are IFN-γ and IL-10.[55] IFN-γ is known to be an early mediator of host response to *M. ulcerans*[56] and increases in patients after 4–8 weeks of antimicrobial treatment, indicating immunocompetence against *M. ulcerans* and the mounting of a supportive CD4+ Th1 response.[55] The

elevated IFN-γ response seen in mice with severe pathology (Figure 3A) can, thus, be interpreted as an early reaction to a large amount of actively multiplying bacteria, whereas at week 17, mice with no pathology had higher IFN-γ levels than those with pathology possibly because of sufficient host control of the pathogen. Consistently, patients with pre-ulcerative lesions (early phase) and patients with healed lesions (host control) both showed elevated IFN-γ levels,[57] whereas IL-10 seems to be somewhat nonspecifically elevated during all phases of BU disease.[52,55,57]

Specific antibody responses were detected within 2 weeks of infection, which increased over the course of the next 4 weeks and were maintained at a consistent level for up 17 weeks. Antibody titers slowly rose, but only at week 8. The decline in photons/s and the increase in antibody titers coincided in weeks 7–8. It is not clear if rising antibody levels helped to gain control of the infection or if declining bacterial load resulted in less immune suppression by ML and led to reactivation of the immune system and increase in antibody levels. In humans, serological screening for Hsp18 antibodies indicates that large parts of the population in endemic areas are exposed to *M. ulcerans*, but only some develop the disease.[58] Guinea pigs infected with *M. ulcerans* appear to self-heal as do some mice.[59] Furthermore, spontaneous loss of the plasmid encoding for the polyketide synthases that produce the *M. ulcerans* toxin ML has been observed in mice. In that case, *M. ulcerans* was rendered nonpathogenic.[60] It is conceivable that humans infected with certain doses of *M. ulcerans* develop either no disease, limited disease, or even unnoticed disease that self-resolves. Evidence for these scenarios has been observed in BU patients who have defaulted from antibiotic treatment regimens, yet could still be contacted for follow-up and showed to have healed lesions despite incomplete treatment.[61] It is likely that the bacterial burden was not zero in these patients at the time of default but that it reached a critical nadir at which host immunity overcame the counteracting effect of ML and controlled infection. Individuals who are able to establish an efficient immune response to MU might control and clear the infection unnoticed as was the case with 50% of subcutaneously infected mice in our experiment. We have previously deduced a low infectious
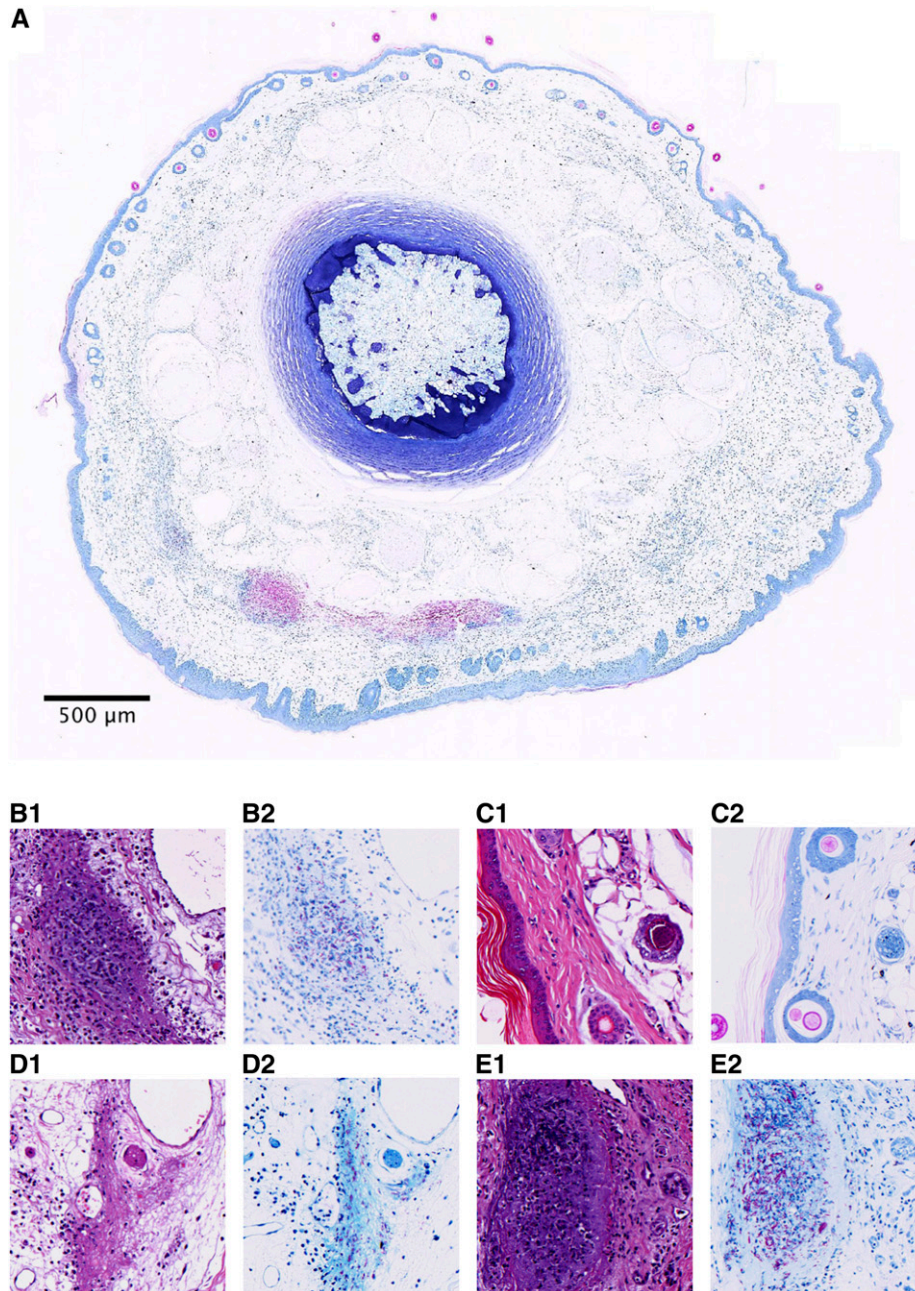
FIGURE 4.   Histological specimens of mice infected with *Mycobacterium ulcerans* into the tail in hematoxylin and eosin (**A1**, **B1**, **C1**, and **D1**) or Ziehl–Neelsen (**A.2**, **B.2**, **C.2**, and **D.2**) staining. (**A**) Whole slide cross-section of mouse tail (ID #85) infected with *M. ulcerans* subcutaneously, humanely killed 8 weeks postinfection because of advanced clinical pathology. Visible are clusters of acid-fast bacilli (AFB) and in the cutis and subcutis, approx. 300–400 μm beneath the surface (**B**.1 and **B**.2). Example of the presence of AFB in mouse 85, as well as granuloma formation (**C**.1 and **C**.2). Normal mouse tail histology of a naive, uninfected mouse with thin epidermis and intact hair follicles. (**D**.1 and **D**.2) Moderate pathology (mouse 89) with diffuse inflammation, tissue damage, and presence of AFB. Involvement of blood vessels with zones of inflammation and also destruction of smaller vessels was visible in this specimen too (vasculopathy) (**E**.1 and **E**.2). Necrosis, granuloma formation, inflammation, and abundant extracellular clustering of AFB were observed in mice with severe pathology (mouse 84). This figure appears in color at www.ajtmh.org.

dose 50% (ID50) of < 10 CFU from experiments involving mechanical injury simulated by needle stick to *M. ulcerans* externally contaminated mouse tails.[10] Even though in this present research, bacterial presence was measured by IVIS imaging in 90% of mice, only 50% of animals showed clinical disease in this experiment following SC injection with approx. 3.3×10^5 CFU/mL. This observation and discrepancy with our previous research might be explained by the different handling of the inoculating needle, perpendicular, and supposedly

deeper penetration in the study by Wallace et al.[10] and more superficial penetration in a 20–30° angle in SC injections in this study. Experiments are required to assess the *M. ulcerans* ID50 using carefully controlled inoculation conditions, perhaps using a micromanipulator with decreasing doses of *M. ulcerans*.

At week 8, three of the infected animals had reached the humane experimental endpoint and were culled. Their cytokine profile data were comparable with those of the other

animals culled at week 17 and provide an insight into the evolution of the cytokine profile. Although there were considerable amounts of IFN-γ and IL-10, indicating a Th1-mediated response observed in the animals sacrificed at week 8, all cytokine levels were reduced by week 17. The suppression of cytokines is due to the inhibition by ML of the nascent membrane, and secretory proteins egress through the endoplasmic reticulum membrane.[6,62] In human patients with BU, overall suppressed IFN-γ levels are seen.[52] The triad of peak bacterial load with worsening pathology, low but rising antibody titers, and elevated Th1 subset cytokines in week 7 could also explain the paradoxical response seen in patients; an overreaction and inflammation of the reactivating immune system noted in patients beginning antibiotics for BU.[63] Animals not showing clinical signs of disease had marginally higher antibody levels against *M. ulcerans* (Figure 2), possibly indicating some sort of immune response to the infection, although the results were statistically not significant in our small sample.

We demonstrated virulence of the *M. ulcerans*+pMV306 hsp16+luxG13 reporter strain and observed localized clinical disease with human-like pathology in 50% of the animals after inoculation with 3.3×10^5 CFU/mL bacteria. There are several limitations to our study. We did not assess CFU counts in the lesions at the disease endpoint; processing of tail sections for histopathology instead to compare histopathology of the bioluminescent strain was prioritized in this early, proof-of-principle study. Previous studies have shown a good correlation between CFU and luminescence in the mouse footpad model, at least for the first 8 weeks of the disease.[31,35] Future studies should reconfirm this relationship with IVIS imaging in a larger experiment. Furthermore, technical inconsistencies, especially while injecting the bacteria into the fine skin of the BALB/c mouse, can also account for different results. The immune parameters measured are not only in line with the previous finding in the literature, as described earlier, but also derived from a small sample size in this experiment. They should, therefore, be understood as a baseline for further studies rather than a basis for the discussion of BU pathology.

We successfully applied IVIS imaging of the bioluminescent *M. ulcerans* JKD8049 (pMV306 hsp16+luxG13) to the murine tail-infection model. We hope that the tool presented here will be used in future research on *M. ulcerans* and aid in preclinical research. We strongly believe that the application of modern, noninvasive in vivo bacterial imaging can reduce and refine animal experimentation in BU research. We will continue to test and validate this model and apply it for the study of BU transmission and vaccination research.

Authors' addresses: Till F. Omansen and Ymkje Stienstra, Department of Internal Medicine/Infectious Diseases, University Medical Center Groningen, University of Groningen, Groningen, The Netherlands, E-mails: t.f.omansen@umcg.nl and y.stienstra@umcg.nl. Renee A. Marcsisin, Brendon Y. Chua, Weiguang Zeng, David C. Jackson, Jessica L. Porter, and Timothy P. Stinear, Department of Microbiology and Immunology, The Peter Doherty Institute for Infection and Immunity, University of Melbourne, Parkville, Australia, E-mails: reneemarcsisin@gmail.com, bychua@unimelb.edu.au, weiguang@ unimelb.edu.au, davidcj@unimelb.edu.au, jlporter@unimelb.edu.au, and tstinear@unimelb.edu.au. Tjip S. van der Werf, Department of Pulmonary Diseases and Tuberculosis, University Medical Center Groningen, University of Groningen, Groningen, The Netherlands, E-mail: t.s.van.der.werf@umcg.nl.

REFERENCES

1. van der Werf TS et al., 2005. *Mycobacterium ulcerans* disease. *Bull World Health Organ 83:* 785–791.
2. WHO, 2019. *Buruli Ulcer Fact Sheet*. Available at: https://www.who.int/news-room/fact-sheets/detail/buruli-ulcer-(mycobacterium-ulcerans-infection). Accessed May 21, 2019.
3. de Zeeuw J et al., 2014. Persisting social participation restrictions among former Buruli ulcer patients in Ghana and Benin. *PLoS Negl Trop Dis 8:* e3303.
4. George KM, Chatterjee D, Gunawardana G, Welty D, Hayman J, Lee R, Small PL, 1999. Mycolactone: a polyketide toxin from *Mycobacterium ulcerans* required for virulence. *Science 283:* 854–857.
5. George KM, Pascopella L, Welty DM, Small PL, 2000. A *Mycobacterium ulcerans* toxin, mycolactone, causes apoptosis in Guinea pig ulcers and tissue culture cells. *Infect Immun 68:* 877–883.
6. Hall BS, Hill K, McKenna M, Ogbechi J, High S, Willis AE, Simmonds RE, 2014. The pathogenic mechanism of the *Mycobacterium ulcerans* virulence factor, mycolactone, depends on blockade of protein translocation into the ER. *PLoS Pathog 10:* e1004061.
7. Demangel C, High S, 2018. Sec61 blockade by mycolactone: a central mechanism in Buruli ulcer disease. *Biol Cell 110:* 237–248.
8. Stinear TP et al., 2004. Giant plasmid-encoded polyketide synthases produce the macrolide toxin of *Mycobacterium ulcerans*. *Proc Natl Acad Sci USA 101:* 1345–1349.
9. Meyers WM, Shelly WM, Connor DH, 1974. Heat treatment of *Mycobacterium ulcerans* infections without surgical excision. *Am J Trop Med Hyg 23:* 924–929.
10. Wallace JR et al., 2017. *Mycobacterium ulcerans* low infectious dose and mechanical transmission support insect bites and puncturing injuries in the spread of Buruli ulcer. *PLoS Negl Trop Dis 11:* e0005553.
11. Johnson PD, Azuolas J, Lavender CJ, Wishart E, Stinear TP, Hayman JA, Brown L, Jenkin GA, Fyfe JA, 2007. *Mycobacterium ulcerans* in mosquitoes captured during outbreak of Buruli ulcer, southeastern Australia. *Emerg Infect Dis 13:* 1653–1660.
12. Lavender CJ, Fyfe JA, Azuolas J, Brown K, Evans RN, Ray LR, Johnson PD, 2011. Risk of Buruli ulcer and detection of *Mycobacterium ulcerans* in mosquitoes in southeastern Australia. *PLoS Negl Trop Dis 5:* e1305.
13. Etuaful S et al., 2005. Efficacy of the combination rifampin-streptomycin in preventing growth of *Mycobacterium ulcerans* in early lesions of Buruli ulcer in humans. *Antimicrob Agents Chemother 49:* 3182–3186.
14. Nienhuis WA et al., 2010. Antimicrobial treatment for early, limited *Mycobacterium ulcerans* infection: a randomised controlled trial. *Lancet 375:* 664–672.
15. Kibadi K et al., 2010. Response to treatment in a prospective cohort of patients with large ulcerated lesions suspected to be Buruli ulcer (Mycobacterium *ulcerans* disease). *PLoS Negl Trop Dis 4:* e736.
16. Wadagni AC, Barogui YT, Johnson RC, Sopoh GE, Affolabi D, van der Werf TS, de Zeeuw J, Kleinnijenhuis J, Stienstra Y, 2018. Delayed versus standard assessment for excision surgery in patients with Buruli ulcer in Benin: a randomised controlled trial. *Lancet Infect Dis 18:* 650–656.
17. Einarsdottir T, Huygen K, 2011. Buruli ulcer. *Hum Vaccin 7:* 1198–1203.
18. Dega H, Robert J, Bonnafous P, Jarlier V, Grosset J, 2000. Activities of several antimicrobials against *Mycobacterium ulcerans* infection in mice. *Antimicrob Agents Chemother 44:* 2367–2372.
19. Bentoucha A, Robert J, Dega H, Lounis N, Jarlier V, Grosset J, 2001. Activities of new macrolides and fluoroquinolones against *Mycobacterium ulcerans* infection in mice. *Antimicrob Agents Chemother 45:* 3109–3112.

20. Dega H, Bentoucha A, Robert J, Jarlier V, Grosset J, 2002. Bactericidal activity of rifampin-amikacin against *Mycobacterium ulcerans* in mice. *Antimicrob Agents Chemother 46:* 3193–3196.

21. Marsollier L, Robert R, Aubry J, Saint André J-P, Kouakou H, Legras P, Manceau AL, Mahaza C, Carbonnelle B, 2002. Aquatic insects as a vector for *Mycobacterium ulcerans*. *Appl Environ Microbiol 68:* 4623–4628.

22. Shepard CC, 1960. The experimental disease that follows the injection of human leprosy bacilli into foot-pads of mice. *J Exp Med 112:* 445–454.

23. Tanghe A, Dangy J-P, Pluschke G, Huygen K, 2008. Improved protective efficacy of a species-specific DNA vaccine encoding mycolyl-transferase Ag85A from *Mycobacterium ulcerans* by homologous protein boosting. *PLoS Negl Trop Dis 2:* e199.

24. Tanghe A, Adnet P-Y, Gartner T, Huygen K, 2007. A booster vaccination with *Mycobacterium bovis* BCG does not increase the protective effect of the vaccine against experimental *Mycobacterium ulcerans* infection in mice. *Infect Immun 75:* 2642–2644.

25. Dhople AM, Namba K, 2003. Activities of sitafloxacin (DU-6859a), either singly or in combination with rifampin, against *Mycobacterium ulcerans* infection in mice. *J Chemother 15:* 47–52.

26. Converse PJ et al., 2018. Shorter-course treatment for *Mycobacterium ulcerans* disease with high-dose rifamycins and clofazimine in a mouse model of Buruli ulcer. *PLoS Negl Trop Dis 12:* e0006728.

27. Converse PJ, Xing Y, Kim KH, Tyagi S, Li S-Y, Almeida DV, Nuermberger EL, Grosset JH, Kishi Y, 2014. Accelerated detection of mycolactone production and response to antibiotic treatment in a mouse model of *Mycobacterium ulcerans* disease. *PLoS Negl Trop Dis 8:* e2618.

28. Sarfo FS, Converse PJ, Almeida DV, Zhang J, Robinson C, Wansbrough-Jones M, Grosset JH, 2013. Microbiological, histological, immunological, and toxin response to antibiotic treatment in the mouse model of *Mycobacterium ulcerans* disease. *PLoS Negl Trop Dis 7:* e2101.

29. Converse PJ, Almeida DV, Nuermberger EL, Grosset JH, 2011. BCG-mediated protection against *Mycobacterium ulcerans* infection in the mouse. *PLoS Negl Trop Dis 5:* e985.

30. Zhang T, Li SY, Converse PJ, Almeida DV, Grosset JH, Nuermberger EL, 2011. Using bioluminescence to monitor treatment response in real time in mice with *Mycobacterium ulcerans* infection. *Antimicrob Agents Chemother 55:* 56–61.

31. Zhang T, Bishai WR, Grosset JH, Nuermberger EL, 2010. Rapid assessment of antibacterial activity against *Mycobacterium ulcerans* by using recombinant luminescent strains. *Antimicrob Agents Chemother 54:* 2806–2813.

32. Almeida D, Converse PJ, Ahmad Z, Dooley KE, Nuermberger EL, Grosset JH, 2011. Activities of rifampin, rifapentine and clarithromycin alone and in combination against *Mycobacterium ulcerans* disease in mice. *PLoS Negl Trop Dis 5:* e933.

33. Almeida DV, Converse PJ, Li S-Y, Tyagi S, Nuermberger EL, Grosset JH, 2013. Bactericidal activity does not predict sterilizing activity: the case of rifapentine in the murine model of *Mycobacterium ulcerans* disease. *PLoS Negl Trop Dis 7:* e2085.

34. Converse PJ, Tyagi S, Xing Y, Li S-Y, Kishi Y, Adamson J, Nuermberger EL, Grosset JH, 2015. Efficacy of rifampin plus clofazimine in a murine model of *Mycobacterium ulcerans* disease. *PLoS Negl Trop Dis 9:* e0003823.

35. Zhang T, Li SY, Converse PJ, Grosset JH, Nuermberger EL, 2013. Rapid, serial, non-invasive assessment of drug efficacy in mice with autoluminescent Mycobacterium *ulcerans* infection. *PLoS Negl Trop Dis 7:* e2598.

36. Coutanceau E, Legras P, Marsollier L, Reysset G, Cole ST, Demangel C, 2006. Immunogenicity of *Mycobacterium ulcerans* Hsp65 and protective efficacy of a *Mycobacterium leprae* Hsp65-based DNA vaccine against Buruli ulcer. *Microbes Infect 8:* 2075–2081.

37. Yerramilli A et al., 2017. The location of Australian Buruli ulcer lesions-implications for unravelling disease transmission. *PLoS Negl Trop Dis 11:* e0005800.

38. Leach RH, Fenner F, 1954. Studies on *Mycobacterium ulcerans* and *Mycobacterium balnei*. *Aust J Exp Biol Med Sci 32:* 835–852.

39. Omansen TF, Porter JL, Johnson PDR, van der Werf TS, Stienstra Y, Stinear TP, 2015. In-vitro activity of avermectins against Mycobacterium *ulcerans*. *PLoS Negl Trop Dis 9:* e0003549.

40. Andreu N et al., 2010. Optimisation of bioluminescent reporters for use with mycobacteria. *PLoS One 5:* e10777.

41. Andreu N, Zelmer A, Sampson SL, Ikeh M, Bancroft GJ, Schaible UE, Wiles S, Robertson BD, 2013. Rapid in vivo assessment of drug efficacy against *Mycobacterium tuberculosis* using an improved firefly luciferase. *J Antimicrob Chemother 68:* 2118–2127.

42. Hong H, Gates PJ, Staunton J, Stinear T, Cole ST, Leadlay PF, Spencer JB, 2003. Identification using LC-MSn of co-metabolites in the biosynthesis of the polyketide toxin mycolactone by a clinical isolate of *Mycobacterium ulcerans*. *Chem Commun (Camb) 22:* 2822–2823.

43. Gooding TM, Johnson PD, Campbell DE, Hayman JA, Hartland EL, Kemp AS, Robins-Browne RM, 2001. Immune response to infection with *Mycobacterium ulcerans*. *Infect Immun 69:* 1704–1707.

44. Pidot SJ et al., 2010. Serological evaluation of *Mycobacterium ulcerans* antigens identified by comparative genomics. *PLoS Negl Trop Dis 4:* e872.

45. Mwanatambwe M, Fukunishi Y, Yajima M, Suzuki K, Asiedu K, Etuafel S, Yamada N, Asano G, 2000. Clinico-histopathological findings of Buruli ulcer. *Nihon Hansenbyo Gakkai Zasshi 69:* 93–100.

46. Ruf M-T, Schütte D, Chauffour A, Jarlier V, Ji B, Pluschke G, 2012. Chemotherapy-associated changes of histopathological features of *Mycobacterium ulcerans* lesions in a Buruli ulcer mouse model. *Antimicrob Agents Chemother 56:* 687–696.

47. Guarner J et al., 2003. Histopathologic features of *Mycobacterium ulcerans* infection. *Emerg Infect Dis 9:* 651–656.

48. Rondini S, Horsfield C, Mensah-Quainoo E, Junghanss T, Lucas S, Pluschke G, 2006. Contiguous spread of *Mycobacterium ulcerans* in Buruli ulcer lesions analysed by histopathology and real-time PCR quantification of mycobacterial DNA. *J Pathol 208:* 119–128.

49. Coutanceau E, Decalf J, Martino A, Babon A, Winter N, Cole ST, Albert ML, Demangel C, 2007. Selective suppression of dendritic cell functions by *Mycobacterium ulcerans* toxin mycolactone. *J Exp Med 204:* 1395–1403.

50. Phillips R, Sarfo FS, Guenin-Macé L, Decalf J, Wansbrough-Jones M, Albert ML, Demangel C, 2009. Immunosuppressive signature of cutaneous *Mycobacterium ulcerans* infection in the peripheral blood of patients with Buruli ulcer disease. *J Infect Dis 200:* 1675–1684.

51. Boulkroun S, Guenin-Macé L, Thoulouze M-I, Monot M, Merckx A, Langsley G, Bismuth G, Di Bartolo V, Demangel C, 2010. Mycolactone suppresses T cell responsiveness by altering both early signaling and posttranslational events. *J Immunol 184:* 1436–1444.

52. Gooding TM, Johnson PDR, Smith M, Kemp AS, Robins-Browne RM, 2002. Cytokine profiles of patients infected with *Mycobacterium ulcerans* and unaffected household contacts. *Infect Immun 70:* 5562–5567.

53. Guenin-Macé L, Carrette F, Asperti-Boursin F, Le Bon A, Caleechurn L, Di Bartolo V, Fontanet A, Bismuth G, Demangel C, 2011. Mycolactone impairs T cell homing by suppressing microRNA control of L-selectin expression. *Proc Natl Acad Sci USA 108:* 12833–12838.

54. Fraga AG, Martins TG, Torrado E, Huygen K, Portaels F, Silva MT, Castro AG, Pedrosa J, 2012. Cellular immunity confers transient protection in experimental Buruli ulcer following BCG or mycolactone-negative Mycobacterium *ulcerans* vaccination. *PLoS One 7:* e33406.

55. Sarfo FS, Phillips RO, Ampadu E, Sarpong F, Adentwe E, Wansbrough-Jones M, 2009. Dynamics of the cytokine response to *Mycobacterium ulcerans* during antibiotic treatment for *M. ulcerans* disease (Buruli ulcer) in humans. *Clin Vaccine Immunol 16:* 61–65.

56. Bieri R, Bolz M, Ruf MT, Pluschke G, 2016. Interferon-γ is a crucial activator of early host immune defense against *Mycobacterium ulcerans* infection in mice. *PLoS Negl Trop Dis 10:* e0004450.

57. Schipper HS, Rutgers B, Huitema MG, Etuaful SN, Westenbrink BD, Limburg PC, Timens W, van der Werf TS, 2007. Systemic

and local interferon-gamma production following *Mycobacterium ulcerans* infection. *Clin Exp Immunol 150:* 451–459.

58. Diaz D, Döbeli H, Yeboah-Manu D, Mensah-Quainoo E, Friedlein A, Soder N, Rondini S, Bodmer T, Pluschke G, 2006. Use of the immunodominant 18-kiloDalton small heat shock protein as a serological marker for exposure to *Mycobacterium ulcerans*. *Clin Vaccine Immunol 13:* 1314–1321.

59. Silva-Gomes R, Marcq E, Trigo G, Gonçalves CM, Longatto-Filho A, Castro AG, Pedrosa J, Fraga AG, 2015. Spontaneous healing of *Mycobacterium ulcerans* lesions in the Guinea pig model. *PLoS Negl Trop Dis 9:* e0004265.

60. Nakanaga K et al., 2018. Naturally occurring a loss of a giant plasmid from *Mycobacterium ulcerans* subsp. *shinshuense* makes it non-pathogenic. *Sci Rep 8:* 8218.

61. Klis S, Kingma RA, Tuah W, van der Werf TS, Stienstra Y, 2016. Clinical outcomes of Ghanaian Buruli ulcer patients who defaulted from antimicrobial therapy. *Trop Med Int Health 21:* 1191–1196.

62. Simmonds RE, Lali FV, Smallie T, Small PLC, Foxwell BM, 2009. Mycolactone inhibits monocyte cytokine production by a posttranscriptional mechanism. *J Immunol 182:* 2194–2202.

63. Nienhuis WA et al., 2012. Paradoxical responses after start of antimicrobial treatment in *Mycobacterium ulcerans* infection. *Clin Infect Dis 54:* 519–526.